
Rupture processes in fiber bundle models

Per C. Hemmer, Alex Hansen, and Srutarshi Pradhan

Department of Physics, Norwegian University of Science and Technology, N-7491
Trondheim, Norway `per.hemmer@ntnu.no` `alex.hansen@ntnu.no`
`pradhan.srutarshi@ntnu.no`

1 Introduction

Fiber bundles with statistically distributed thresholds for breakdown of individual fibers are interesting models of the statics and dynamics of failures in materials under stress. They can be analyzed to an extent that is not possible for more complex materials. During the rupture process in a fiber bundle avalanches, in which several fibers fail simultaneously, occur. We study by analytic and numerical methods the statistics of such avalanches, and the breakdown process for several models of fiber bundles. The models differ primarily in the way the extra stress caused by a fiber failure is redistributed among the surviving fibers.

When a rupture occurs somewhere in an elastic medium, the stress elsewhere is increased. This may in turn trigger further ruptures, which can cascade to a final complete breakdown of the material. To describe or model such breakdown processes in detail for a real material is difficult, due to the complex interplay of failures and stress redistributions. Few analytic results are available, so computer simulations is the main tool (See Refs. [1], [2] and [3] for reviews). Fiber bundle models, on the other hand, are characterized by simple geometry and clear-cut rules for how the stress caused by a failed element is redistributed on the intact fibers. The attraction and interest of these models lies in the possibility of obtaining exact results, thereby providing inspiration and reference systems for studies of more complicated materials.

In this review we survey theoretical and numerical results for several models of bundles of N elastic and parallel fibers, clamped at both ends, with statistically distributed thresholds for breakdown of individual fibers (Fig. 1). The individual thresholds x_i are assumed to be independent random variables with the same cumulative distribution function $P(x)$ and a corresponding density function $p(x)$:

$$\text{Prob}(x_i < x) = P(x) = \int_0^x p(u) du. \quad (1)$$

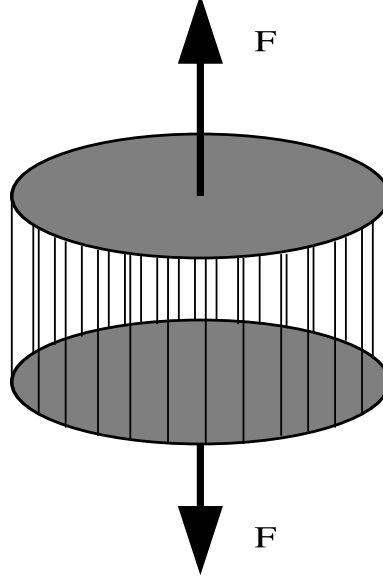


Fig. 1. A fiber bundle of N parallel fibers clamped at both ends. The externally applied force is F .

Whenever a fiber experiences a force equal to or greater than its strength threshold x_i , it breaks immediately and does not contribute to the strength of the bundle thereafter. The maximal load the bundle can resist before complete breakdown of the whole bundle is called the *critical* load. The models differ in the probability distribution of the thresholds. Two popular examples of threshold distributions are the uniform distribution

$$P(x) = \begin{cases} x/x_r & \text{for } 0 \leq x \leq x_r \\ 1 & \text{for } x > x_r, \end{cases} \quad (2)$$

and the Weibull distribution

$$P(x) = 1 - \exp(-(x/x_r)^k). \quad (3)$$

Here $x \geq 0$, x_r is a reference threshold and the dimensionless number k is the Weibull index (Fig. 2).

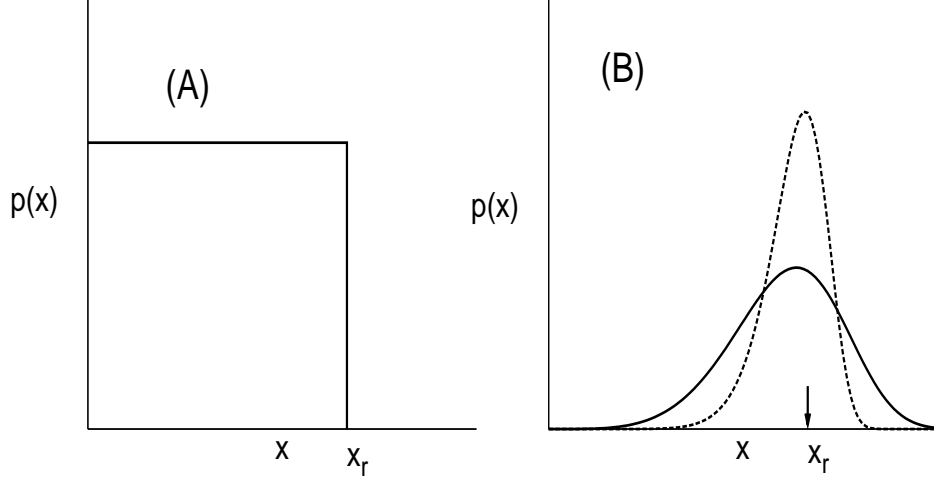


Fig. 2. The uniform distribution (A) and Weibull distributions (B) with $k = 5$ (solid line) and $k = 10$ (dotted line).

Much more fundamental, however, is the way the models differ in the mechanism for how the extra stress caused by a fiber failure is redistributed among the unbroken fibers. The simplest models are the equal-load-sharing models, in which the load previously carried by a failed fiber is shared equally by all the remaining intact bonds in the system. That some exact results could be extracted for this model was demonstrated by Daniels [4] in a classic work some sixty years ago. Local-load-sharing models, on the other hand, are relevant for materials in which the load originally carried by a failed fiber is shared by the surviving fibers in the immediate vicinity of the ruptured fiber.

The main property of the fiber bundle breakdown process to be studied in the present review is the distribution of the sizes of the burst avalanches. The *burst distribution* $D(\Delta)$ is defined as the expected number of bursts in which Δ fibers break simultaneously when the bundle is stretched until complete breakdown. For the equal-load-distribution models that we consider in Sec. 2 Hemmer and Hansen [5] showed that the generic result is a power law,

$$\lim_{N \rightarrow \infty} \frac{D(\Delta)}{N} \propto \Delta^{-\xi}, \quad (4)$$

for large Δ , with $\xi = 5/2$. In Sec. 2.2 we will show, however, that for some rather unusual threshold distributions the power law (4) is not obeyed. More importantly, we show in Sec. 2.4 that when the whole bundle at the outset is close to being critical, the exponent ξ crosses over to the value $\xi = 3/2$. In Sec. 2.5 we pay particular attention to the rupture process at criticality, *i.e.*, just before the whole bundle breaks down.

The average strength of the bundle for a given load can be viewed as the result of a sequential process. In the first step all fibers that cannot withstand the applied load break. Then the stress is redistributed on the surviving fibers, which compels further fibers to burst. This starts an iterative process that continues until equilibrium is reached, or all fibers fail. When equilibrium exists, it characterizes the *average* strength of the bundle for the given load. This recursive dynamics can be viewed as a fixed-point problem, with interesting properties when the critical load is approached. We review such recursive dynamics in Sec. 2.6.

For other stress redistribution principles than equal-load-sharing, the avalanche distributions are different from the power law (4). In Sec. 3 we study examples of such systems. Special cases are local-stress-distribution models in which the surviving nearest neighbors to a failed fiber share all the extra stress, and a model in which the fibers are anchored to an elastic clamp.

2 Equal-load-sharing fiber bundles

This is the fiber-bundle model with the longest history. It was used by Pierce, in the context of testing the strength of cotton yarn [6]. The basic assumptions are that the fibers obey Hookean elasticity right up to the breaking point, and that the load distributes itself *evenly* among the surviving fibers. The model with this democratic load redistribution is similar to mean-field models in statistical physics.

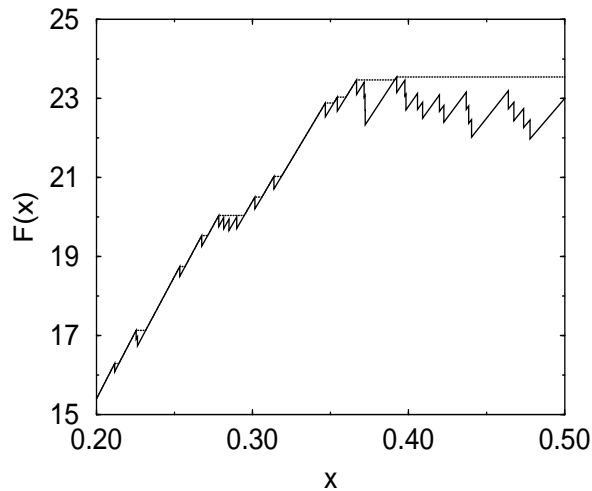


Fig. 3. $F(x)$ vs. x curve. Avalanches are shown as horizontal lines.

At a force x per surviving fiber, the total force on the bundle is

$$F(x) = Nx[1 - \phi(x)] , \quad (5)$$

where $\phi(x)$ is the fraction of failed fibers. In Fig. 3 we show an example of a F vs. x . We have in mind an experiment in which the force F , our control parameter (Fig. 1), is steadily increasing. This implies that not all parts of the $F(x)$ curve are physically realized. The experimentally relevant function is

$$F_{ph}(x) = \text{LMF } F(x) , \quad (6)$$

the least monotonic function not less than $F(x)$. A horizontal part of $F_{ph}(x)$ corresponds to an avalanche, the size of which is characterized by the number of maxima of $F(x)$ within the corresponding range of x (Fig. 3).

It is the fluctuations in $F(x)$ that create avalanches. For a large sample the fluctuations will be small deviations from the average macroscopic characteristics $\langle F \rangle$. This *average* total force is given by

$$\langle F \rangle(x) = Nx[1 - P(x)]. \quad (7)$$

Let us for the moment assume that $\langle F \rangle(x)$ has a single maximum. The maximum corresponds to the value $x = x_c$ for which $d\langle F \rangle/dx$ vanishes. This gives

$$1 - P(x_c) - x_c p(x_c) = 0. \quad (8)$$

The threshold x_c corresponding to the maximum of F is denoted the *critical* threshold. Because of fluctuations, however, the maximum value of the force may actually occur at a slightly different value of x .

2.1 Burst distribution: The generic case.

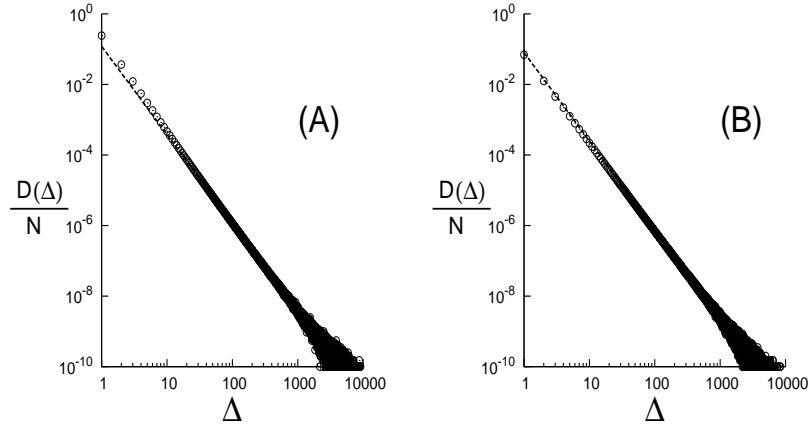


Fig. 4. The burst distribution $D(\Delta)/N$ for the uniform distribution (A) and the Weibull distribution with index 5 (B). The dotted lines represent the power law with exponent $-5/2$. Both figures are based on 20000 samples of bundles each with $N = 10^6$ fibers.

That the rupture process produces a power-law decay of the burst distribution $D(\Delta)$ is seen at once by simulation experiments. Fig. 4 shows results for the uniform threshold distribution (2) and the Weibull distribution (3) with index $k = 5$.

In order to derive analytically the burst distribution, let us start by considering a small threshold interval $(x, x + dx)$ in a range where the average force $\langle F \rangle(x)$ increases with x . For a large number N of fibers the expected number of surviving fibers is $N[1 - P(x)]$. And the threshold values in the interval, of which there are $Np(x)dx$, will be Poisson distributed. When N is arbitrarily large, the burst sizes can be arbitrarily large in any finite interval of x .

Assume that an infinitesimal increase in the external force results in a break of a fiber with threshold x . Then the load that this fiber suffered, will be redistributed on the $N[1 - P(x)]$ remaining fibers; thus they experience a load increase

$$\delta x = \frac{x}{N[1 - P(x)]}. \quad (9)$$

The *average* number of fibers that break as a result of this load increase is

$$a = a(x) = Np(x) \cdot \delta x = \frac{xp(x)}{1 - P(x)}. \quad (10)$$

For a burst of size Δ the increase in load per fiber will be a factor Δ larger than the quantity (9), and an average number $a(x)\Delta$ will break. The probability that precisely $\Delta - 1$ fibers break as a consequence of the first failure is given by a Poisson distribution with this average, i.e. it equals

$$\frac{(a\Delta)^{\Delta-1}}{(\Delta-1)!} e^{-a\Delta}. \quad (11)$$

This is not sufficient, however. We must ensure that the thresholds for these $\Delta - 1$ fibers are not so high that the avalanche stops before reaching size Δ . This requires that at least n of the thresholds are in the interval $(x, x + n\delta x)$, for $1 \leq n \leq \Delta - 1$. In other words, if we consider the Δ intervals $(x, x + \delta x)$, $(x + \delta x, x + 2\delta x)$, \dots , $(x + (\Delta - 1)\delta x, x + \Delta\delta x)$, we must find at most $n - 1$ thresholds in the n last intervals. There is the same a priori probability to find a threshold in any interval. The solution to this combinatorial problem is given in Ref. [7]. The resulting probability to find all intermediate thresholds weak enough equals $1/\Delta$. Combining this with (11), we have for the probability $\phi(\Delta, x)$ that the breaking of the first fiber results in a burst of size Δ :

$$\phi(\Delta, x) = \frac{\Delta^{\Delta-1}}{\Delta!} a(x)^{\Delta-1} e^{-a(x)\Delta}. \quad (12)$$

This gives the probability of a burst of size Δ , as a consequence of a fiber burst due to an infinitesimal increase in the external load. However, we still have to ensure that the burst actually *starts* with the fiber in question and

is not part of a larger avalanche starting with another, weaker, fiber. Let us determine the probability $P_b(x)$ that this initial condition is fulfilled.

For that purpose consider the $d-1$ fibers with the largest thresholds below x . If there is no strength threshold in the interval $(x-\delta x, x)$, at most one threshold value in the interval $(x-2\delta x, x)$, ... , at most $d-1$ values in the interval $(x-d\delta x, x)$, then the fiber bundle can not at any of these previous x -values withstand the external load that forces the fiber with threshold x to break. The probability that there are precisely h fiber thresholds in the interval $(x-\delta x, x)$ equals

$$\frac{(ad)^h}{h!} e^{-ad}.$$

Dividing the interval into d subintervals each of length δx , the probability $p_{h,d}$ that these conditions are fulfilled is exactly given by $p_{h,d} = 1 - h/d$ (See Ref. [7]). Summing over the possible values of h , we obtain the probability that the avalanche can not have started with the failure of a fiber with any of the d nearest-neighbor threshold values below x :

$$P_b(x|d) = \sum_{h=0}^{d-1} \frac{(ad)^h}{h!} e^{-ad} \left(1 - \frac{h}{d}\right) = (1-a)e^{-ad} \sum_{h=0}^{d-1} \frac{(ad)^h}{h!} + \frac{(ad)^d}{d!} e^{-ad}. \quad (13)$$

Finally we take the limit $d \rightarrow \infty$, for which the last term vanishes. For $a > 1$ the sum must vanish since the left-hand side of (13) is non-negative, while the factor $(1-a)$ is negative. For $a < 1$, on the other hand, we find

$$P_b(x) = \lim_{d \rightarrow \infty} P_b(x|d) = 1 - a, \quad (14)$$

where $a = a(x)$. The physical explanation of the different behavior for $a > 1$ and $a \leq 1$ is straightforward: The maximum of the total force on the bundle occurs at x_c for which $a(x_c) = 1$, see Eqs. (8) and (10), so that $a(x) > 1$ corresponds to x values almost certainly involved in the final catastrophic burst. The region of interest for us is therefore when $a(x) \leq 1$, where avalanches on a microscopic scale occur. This is accordance with what we found in the beginning of this section, viz. that the burst of a fiber with threshold x leads immediately to a average number $a(x)$ of additional failures.

Summing up, we obtain the probability that the fiber with threshold x is the first fiber in an avalanche of size Δ as the product

$$\Phi(x) = \phi(\Delta, x) P_b(x) = \frac{\Delta^{\Delta-1}}{\Delta!} a(x)^{\Delta-1} e^{-a(x)\Delta} [1 - a(x)], \quad (15)$$

where $a(x)$ is given by Eq. (10),

$$a(x) = \frac{x p(x)}{1 - P(x)}.$$

Since the number of fibers with threshold values in $(x, x+\delta x)$ is $N p(x) dx$, the burst distribution is given by

$$\frac{D(\Delta)}{N} = \frac{1}{N} \int_0^{x_c} \Phi(x) p(x) dx = \frac{\Delta^{\Delta-1}}{\Delta!} \int_0^{x_c} a(x)^{\Delta-1} e^{-a(x)\Delta} [1 - a(x)] p(x) dx. \quad (16)$$

For large Δ the maximum contribution to the integral comes from the neighborhood of the upper integration limit, since $a(x) e^{-a(x)\Delta}$ is maximal for $a(x) = 1$, i.e. for $x = x_c$. Expansion around the saddle point, using

$$a^\Delta e^{-a\Delta} = \exp \left[\Delta \left(-1 - \frac{1}{2}(1-a)^2 + \mathcal{O}(1-a)^3 \right) \right], \quad (17)$$

as well as $a(x) \simeq 1 + a'(x_c)(x - x_c)$, produces

$$\frac{D(\Delta)}{N} = \frac{\Delta^{\Delta-1} e^{-\Delta}}{\Delta!} a'(x_c) \int_0^{x_c} p(x_c) e^{-a'(x_c)^2 (x_c - x)^2 \Delta/2} (x - x_c) dx. \quad (18)$$

The integration yields the asymptotic behavior

$$D(\Delta)/N \propto \Delta^{-\frac{5}{2}}, \quad (19)$$

universal for those threshold distributions for which the assumption of a single maximum of $\langle F \rangle(x)$ is valid.

Note that if the experiment had been stopped before complete breakdown, at a force per fiber x less than x_c , the asymptotic behavior would have been dominated by an *exponential* fall-off rather than a power law:

$$D(\Delta)/N \propto \Delta^{-\frac{5}{2}} e^{-[a(x)-1-\ln a(x)]\Delta}. \quad (20)$$

When x is close to x_c the exponent is proportional to $(x_c - x)^2 \Delta$. The burst distribution then takes the scaling form

$$D(\Delta) \propto \Delta^{-\eta} G(\Delta^\nu (x_c - x)), \quad (21)$$

with a Gaussian function G , a power law index $\eta = \frac{5}{2}$ and $\nu = \frac{1}{2}$. Thus the breakdown process is similar to critical phenomena with a critical point at total breakdown [5, 8, 27].

2.2 Burst distribution: Nongeneric cases

What happens when the average strength curve, $\langle F \rangle(x)$, does *not* have a unique maximum? There are two possibilities: (i) it has *several* parabolic maxima, or (ii) it has *no* parabolic maxima.

When there are several parabolic maxima, and the absolute maximum does not come first (i.e. at the lowest x value), then there will be several avalanche series each terminating at a local critical point with an accompanying burst of macroscopic size, while the breakdown of the bundle occurs when the absolute maximum is reached [9]. The power law asymptotics (19) of the avalanche distribution is thereby unaffected, however.

The second possibility, that the average strength curve has no parabolic maxima, is more interesting. We present here two model examples of such threshold distributions.

The threshold distribution for model I is, in dimensionless units,

$$P(x) = \begin{cases} 0 & \text{for } x \leq 2 \\ 1 - (x - 1)^{-1/2} & \text{for } x > 2, \end{cases} \quad (22)$$

while model II corresponds to

$$P(x) = \begin{cases} 0 & \text{for } x \leq 1 \\ 1 - x^{-\alpha} & \text{for } x > 1, \end{cases} \quad (23)$$

with a positive parameter α .

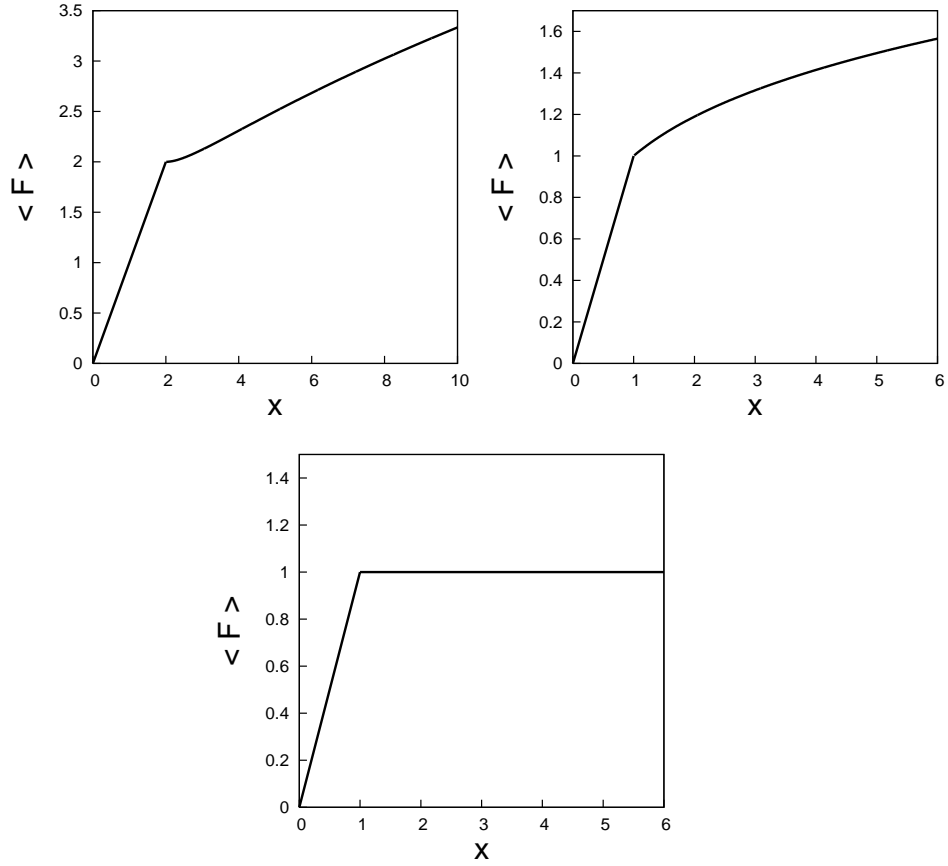


Fig. 5. Average force on the fiber bundle for model I (upper left), model II for $\alpha = 3/4$ (upper right), and model II in the limit $\alpha \rightarrow 1$ (bottom figure).

For the two models the corresponding macroscopic bundle strength per fiber is, according to Eq. (16),

$$\frac{\langle F \rangle}{N} = \begin{cases} x & \text{for } x \leq 2 \\ \frac{x}{\sqrt{x-1}} & \text{for } x > 2 \end{cases} \quad (24)$$

for model I, and

$$\frac{\langle F \rangle}{N} = \begin{cases} x & \text{for } x \leq 1 \\ x^{1-\alpha} & \text{for } x > 1 \end{cases} \quad (25)$$

for model II (see Fig. 5).

To calculate the avalanche distribution we use (16), in both cases with $x_c = \infty$ as the upper limit in the integration. For Model I the $\langle F \rangle$ graph has at $x = 2+$ an extremum, viz. a minimum. At the minimum we have $a(x) = \frac{x}{2(x-1)} = 1$. Since the Δ -dependent factor $a^\Delta e^{-a\Delta}$ in the integrand of (16) has a maximum for $a = 1$, we obtain

$$D(\Delta)/N \propto \Delta^{-5/2} \quad (26)$$

for large Δ . Even if the macroscopic load curve does not have a maximum at any finite x in this case, the generic power law (19) holds.

For model II equation (16) gives

$$\frac{D(\Delta)}{N} = \frac{1-\alpha}{\alpha} \frac{\Delta^{\Delta-1}}{\Delta!} [\alpha e^{-\alpha}]^\Delta \propto \Delta^{-\frac{3}{2}} [\alpha e^{1-\alpha}]^\Delta. \quad (27)$$

For $\alpha = 3/4$ as in Fig. 5, or more generally $\alpha < 1$, the avalanche distribution does *not* follow a power law, but has an exponential cut-off in addition to a $\Delta^{-3/2}$ dependence.

When $\alpha \rightarrow 1$, the average force (25) approaches a constant for $x > 1$, and the burst distribution (27) approaches a power law

$$\frac{D(\Delta)}{N} \propto \Delta^{-3/2}, \quad (28)$$

a result easily verified by simulation on the system with $P(x) = 1 - 1/x$ for $x \geq 1$. That a power law with exponent $3/2$, different from the generic burst distribution (19), appears when

$$\frac{d}{dx} \langle F \rangle \rightarrow 0, \quad (29)$$

will be apparent when we in Sec. 2.5 study what happens at criticality.

2.3 Mapping onto a random walk problem

Let F_k be the force on the bundle when the k th fiber fails. It is the nonmonotonicities in the sequence F_1, F_2, \dots that produce avalanches of size $\Delta > 1$. Let us consider the probability distribution of the force increase $\Delta F = F_{k+1} - F_k$ between two consecutive bursts, the first taking place at a force $x = x_k$ per fiber, so that $F_k = (N - k + 1)x$.

Since $\Delta F = (N - k)(x_{k+1} - x) - x$, it follows that

$$\Delta F \geq -x. \quad (30)$$

The probability to find the $k + 1$ th threshold in the interval $(x_{k+1}, x_{k+1} + dx_{k+1})$, for given $x = x_k$, equals

$$(N - k - 1) \frac{[1 - P(x_{k+1})]^{N-k-2}}{[1 - P(x)]^{N-k-1}} p(x_{k+1}) dx_{k+1}. \quad (31)$$

By use of the connection $x_{k+1} = x + (\Delta F + x)/(N - k)$ this probability density for x_{k+1} is turned into the probability density $\rho(\Delta F) d\Delta F$ for ΔF :

$$\rho(\Delta F) = \frac{N - k - 1}{N - k} \frac{[1 - P(x + (\Delta F + x)/(N - k))]^{N-k-2}}{[1 - P(x)]^{N-k-1}} p\left(x + \frac{\Delta F + x}{N - k}\right), \quad (32)$$

which is properly normalized to unity. For large $N - k$ this simplifies to

$$\rho(\Delta F) = \begin{cases} 0 & \text{for } \Delta F < -x \\ \frac{p(x)}{1 - P(x)} \exp\left[-\frac{(\Delta F + x)}{1 - P(x)} p(x)\right] & \text{for } \Delta F \geq -x. \end{cases} \quad (33)$$

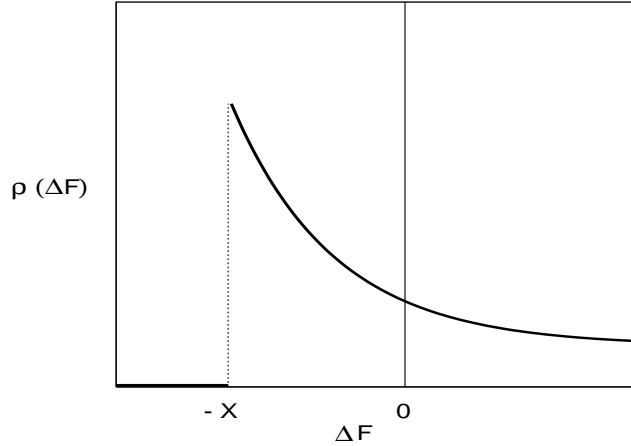


Fig. 6. The probability distribution $\rho(\Delta F)$ of the step length in the random walk.

The values $F_1, F_2, F_3 \dots$ of the force on the bundle can be considered as the positions of a random walker with the probability $\rho(\Delta F)$ for the length of

the next step [8]. It is a random walk of an unusual type: The step length is variable, with the steps in the negative direction are limited in size (Fig. 6). In general the walk is *biased* since

$$\langle \Delta F \rangle = \int \Delta F \rho(\Delta F) d\Delta F = \frac{1 - P(x) - xp(x)}{p(x)} \quad (34)$$

is zero, *e.g.* unbiased, *only* at the critical threshold x_c , given by Eq. (8). That the random walk is unbiased at criticality is to be expected, of course, since the average bundle strength $\langle F \rangle$ as function of x is stationary here.

The probability that ΔF is positive equals

$$\text{Prob}(\Delta F > 0) = \int_0^\infty \rho(\Delta F) d\Delta F = \exp \left[-\frac{xp(x)}{1 - P(x)} \right]. \quad (35)$$

That ΔF is positive implies that the burst has the length $\Delta = 1$. The result (35) is identical to the previously determined probability $\phi(1, x)$, (12), for a burst of length 1, when we have not ensured that the burst actually *starts* with the fiber in question and is not part of a larger avalanche.

In section 2.5 we will see that the random-walk analogy can be used in a quantitative way to predict the avalanche distribution power-law exponent at criticality.

2.4 Crossover behavior near criticality

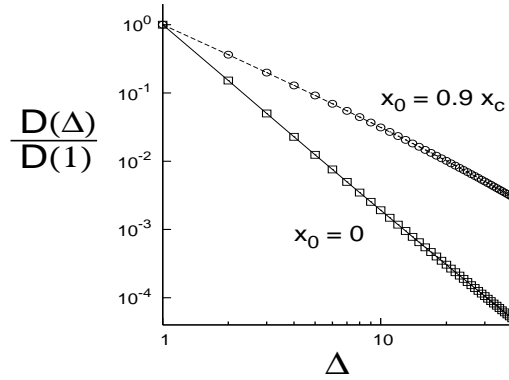


Fig. 7. The distribution of bursts for threshold's uniformly distributed in an interval (x_0, x_c) , with $x_0 = 0$ and with $x_0 = 0.9x_c$. The figure is based on 50 000 samples, each with $N = 10^6$ fibers.

When *all* fiber failures are recorded we have seen that the burst distribution $D(\Delta)$ follows the asymptotic power law $D \propto \Delta^{-5/2}$. If we just sample bursts that occur near criticality, a different behavior is seen [10, 11]. As an illustration we consider the uniform threshold distribution, and compare

the complete burst distribution with what one gets when one samples merely bursts from breaking fibers in the threshold interval $(0.9x_c, x_c)$. Fig. 7 shows clearly that in the latter case a different power law is seen.

If we want to study specifically the contribution from failures occurring when the bundle is nearly critical, we evaluate the expression (18) for the burst distribution over a small interval (x_0, x_c) , rather than integrating from 0 to x_c . The argument in Sec. 2.1 that the major contribution to the integral comes from the critical neighborhood is still valid. We obtain

$$\frac{D(\Delta)}{N} = \frac{\Delta^{\Delta-2} e^{-\Delta}}{\Delta!} \frac{p(x_c)}{a'(x_c)} \left[1 - e^{-\Delta/\Delta_c} \right], \quad (36)$$

with

$$\Delta_c = \frac{2}{a'(x_c)^2 (x_c - x_0)^2}. \quad (37)$$

By use of Stirling approximation $\Delta! \simeq \Delta^\Delta e^{-\Delta} \sqrt{2\pi\Delta}$, – a reasonable approximation even for small Δ – the burst distribution (36) may be written

$$\frac{D(\Delta)}{N} = C \Delta^{-5/2} \left(1 - e^{-\Delta/\Delta_c} \right), \quad (38)$$

with a nonzero constant

$$C = (2\pi)^{-1/2} p(x_c)/a'(x_c). \quad (39)$$

We see from (38) that there is a crossover at a burst length around Δ_c , so that

$$\frac{D(\Delta)}{N} \propto \begin{cases} \Delta^{-3/2} & \text{for } \Delta \ll \Delta_c \\ \Delta^{-5/2} & \text{for } \Delta \gg \Delta_c \end{cases} \quad (40)$$

The difference between the two power-law exponents is unity, as suggested by Sornette’s “sweeping of an instability” mechanism [12]. Such a difference in avalanche power law exponents has been observed numerically by Zapperi et al. in a fuse model [13].

We have thus shown the existence of a crossover from the generic asymptotic behavior $D \propto \Delta^{-5/2}$ to the power law $D \propto \Delta^{-3/2}$ near criticality, i.e., near global breakdown. The crossover is a universal phenomenon, independent of the threshold distribution $p(x)$. In addition we have located where the crossover takes place.

For the uniform distribution $\Delta_c = (1 - x_0/x_c)^{-2}/2$, so for $x_0 = 0.8x_c$, we have $\Delta_c = 12.5$. For the Weibull distribution $P(x) = 1 - \exp(-(x-1)^{10})$, where $1 \leq x \leq \infty$, we get $x_c = 1.72858$ and for $x_0 = 1.7$, the crossover point will be at $\Delta_c \simeq 14.6$. Such crossover is clearly observed (Fig. 8) near the expected values $\Delta = \Delta_c = 12.5$ and $\Delta = \Delta_c = 14.6$, respectively, for the above distributions.

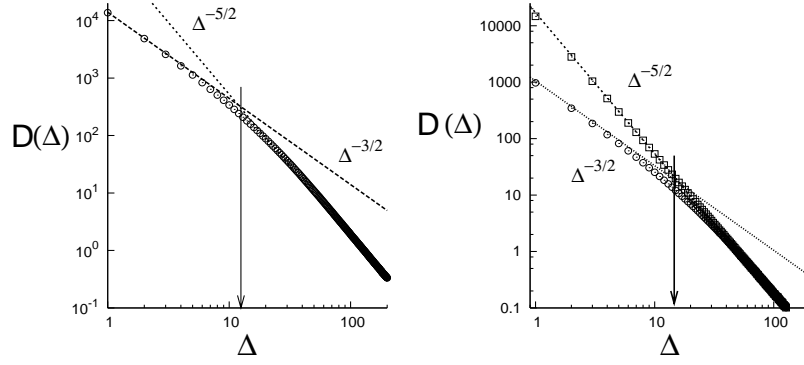


Fig. 8. The distribution of bursts for the uniform threshold distribution (left) with $x_0 = 0.80x_c$ and for a Weibull distribution (right) with $x_0 = 1$ (square) and $x_0 = 1.7$ (circle). Both the figures are based on 50000 samples with $N = 10^6$ fibers each. The straight lines represent two different power laws, and the arrows locate the crossover points $\Delta_c \simeq 12.5$ and $\Delta_c \simeq 14.6$, respectively.

The simulation results shown in the figures are based on *averaging* over a large number of fiber bundles with moderate N . For applications it is important that crossover signals are seen also in a single sample. We show in Fig. 9 that equally clear power laws are seen in a *single* fiber bundle when N is large.

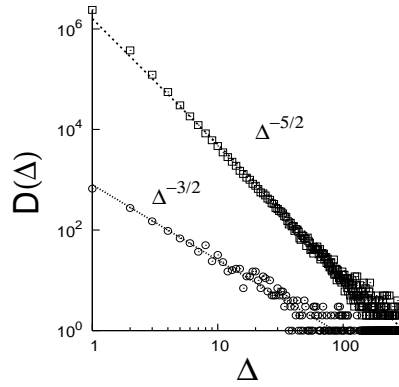


Fig. 9. The distribution of bursts for the uniform threshold distribution for a single fiber bundle with 10^7 fibers. Results with $x_0 = 0$ (recording all avalanches), are shown as squares, the circles stand for avalanches near the critical point ($x_0 = 0.9x_c$).

An important question in strength considerations of materials is how to obtain signatures that can warn of imminent system failure. This is of uttermost importance in, *e.g.*, the diamond mining industry where sudden failure of

the mine can be very costly in terms of lives. These mines are under continuous acoustic surveillance, but at present there are no tell-tale acoustic signature of imminent catastrophic failure. The same type of question is of course also central to earthquake prediction. The crossover seen here in our fiber bundle models is such a signature, it signals that catastrophic failure is imminent. The same type of crossover phenomenon is also seen in the burst distribution of a two-dimensional model of fuses with stochastically distributed current thresholds [10]. This signal does not hinge on observing rare events, and is seen also in a single system (Fig. 9). It has, therefore, a strong potential as a useful detection tool. It is interesting that most recently, Kawamura [14] has observed a decrease in exponent value of the local magnitude distribution of earthquakes as the mainshock is approached (See Fig. 20 of Ref.[14]), analysing earthquakes in Japan (from JUNE catalog).

Obviously, one cannot count bursts all the way to complete breakdown to have a useful detection tool. It suffices to sample bursts in finite intervals (x_0, x_f) , with $x_f < x_c$. In this case we obtain the avalanche distribution by restricting the integration in Eq.(18) to the appropriate intervals. When such an interval is in the neighborhood of x_c we obtain

$$\frac{D(\Delta)}{N} \simeq \frac{\Delta^{\Delta-1} e^{-\Delta} p(x_c) a'(x_c)}{\Delta!} \int_{x_0}^{x_f} e^{-a'(x_c)^2 (x_c-x)^2 \Delta/2} (x - x_c) dx \quad (41)$$

$$\propto \Delta^{-5/2} \left(e^{-\Delta(x_c-x_f)^2/a} - e^{-\Delta(x_c-x_0)/a} \right), \quad (42)$$

with $a = 2/a'(x_c)^2$. This shows a crossover:

$$\frac{D(\Delta)}{N} \propto \begin{cases} \Delta^{-3/2} & \text{for } \Delta \ll a/(x_c - x_0)^2 \\ \Delta^{-5/2} & \text{for } a/(x_c - x_0)^2 \ll \Delta \ll a/(x_c - x_f)^2, \end{cases} \quad (43)$$

with a final exponential behavior when $\Delta \gg a/(x_c - x_f)^2$.

The $3/2$ power law will be seen only when the beginning of the interval, x_0 , is close enough to the critical value x_c . Observing the $3/2$ power law is therefore a signal of imminent system failure.

2.5 Avalanche distribution at criticality

Precisely *at* criticality ($x_0 = x_c$) the crossover takes place at $\Delta_c = \infty$, and consequently the $\xi = 5/2$ power law is no longer present. We will now argue, using the random walk representation in section 2.3, that precisely at criticality the avalanche distribution follows a power law with exponent $3/2$.

At criticality the distribution (33) of the step lengths in the random walk simplifies to

$$\rho_c(\Delta F) = \begin{cases} 0 & \text{for } \Delta F < -x_c \\ x_c^{-1} e^{-1} e^{-\Delta F/x_c} & \text{for } \Delta F \geq -x_c \end{cases} \quad (44)$$

A first burst of size Δ corresponds to a random walk in which the position after each of the first $\Delta-1$ steps is *lower* than the starting point, but after step no. Δ the position of the walker exceeds the starting point. The probability of this equals

$$\text{Prob}(\Delta) = \int_{-x_c}^0 \rho_c(\delta_1) d\delta_1 \int_{x_c}^{-\delta_1} \rho_c(\delta_2) d\delta_2 \int_{-x_c}^{-\delta_1-\delta_2} \rho_c(\delta_3) d\delta_3 \dots \int_{-x_c}^{-\delta_1-\delta_2-\dots-\delta_{\Delta-2}} \rho_c(\delta_{\Delta-1}) d\delta_{\Delta-1} \int_{-\delta_1-\delta_2-\dots-\delta_{\Delta-1}}^{\infty} \rho_c(\delta_{\Delta}) d\delta_{\Delta} \quad (45)$$

To simplify the notation we have introduced $\delta_n \equiv \Delta F_n$. In Ref. [11] we have evaluated the multiple integral (45), with the result

$$\text{Prob}(\Delta) = \frac{\Delta^{\Delta-1} e^{-\Delta}}{\Delta!} \simeq \frac{1}{\sqrt{2\pi}} \Delta^{-3/2}. \quad (46)$$

We note in passing that for the standard unbiased random walk with constant step length we obtain a *different* expression for the burst probability, but again with a $3/2$ power law for large Δ :

$$\text{Prob}(\Delta) = \frac{1}{2^{\Delta-1} \Delta} \left(\frac{\Delta-2}{\frac{1}{2}\Delta-1} \right) \simeq \frac{1}{\sqrt{2\pi}} \Delta^{-3/2}. \quad (47)$$

At completion of the first burst, the force, i.e., the excursion of the random walk, is larger than all previous values. Therefore one may use this point as a new starting point to find, by the same calculation, the distribution of the next burst, etc. Consequently the complete burst distribution is essentially proportional to $\Delta^{-3/2}$, as expected. The simulation results exhibited in Fig. 10 are in excellent agreement with these predictions.

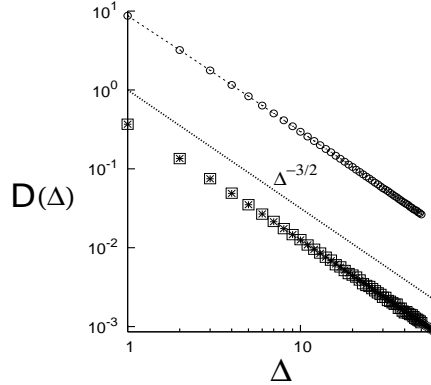


Fig. 10. Distributions of the first bursts (squares) and of all bursts (circles) for the uniform threshold distribution with $x_0 = x_c$. The simulation results are based on 10^6 samples with 80000 fibers each. The crosses stand for the analytic result (46).

One of the unusual threshold distributions we studied in Sec. 2.2 corresponded to an constant average force, $\langle F \rangle/N$ independent of x . Such a bundle is not critical at a single point x_c , but in a whole interval of x . That the burst exponent for this model takes the critical value $3/2$ is therefore no surprise.

2.6 Recursive dynamics

The relation between the number of ruptured fibers and a given external load per fiber, $\sigma = F/N$, can be viewed as the result of a sequential process. In the first step all fibers with thresholds less than $x_1 = \sigma$ must fail. Then the load is redistributed on the surviving fibers, which forces more fibers to burst, etc. This starts an iterative process that goes on until equilibrium is reached, or all fibers rupture [16, 17, 18].

Assume all fibers with thresholds less than x_t break in step number t . The expected number of intact fibers is then

$$U_t = 1 - P(x_t), \quad (48)$$

so that the load per fiber is increased to σ/U_t . In step number $t+1$, therefore, all fibers with threshold less than

$$x_{t+1} = \frac{\sigma}{1 - P(x_t)} \quad (49)$$

must fail. This iteration defines the recursive dynamics [16, 17, 18]. Alternatively an iteration for the U_t can be set up:

$$U_{t+1} = 1 - P(\sigma/U_t); \quad U_0 = 1. \quad (50)$$

If the iteration (49) converges to a finite fixed-point x^* ,

$$\lim_{t \rightarrow \infty} x_t = x^*,$$

the fixed-point value must satisfy

$$x^* = \frac{\sigma}{1 - P(x^*)}. \quad (51)$$

This fixed-point relation,

$$\sigma = x^* [1 - P(x^*)], \quad (52)$$

is identical to the relation (7) between the average force per fiber, $\langle F \rangle/N$, and the threshold value x .

Eq. (52) shows that a necessary condition to have a finite positive fixed-point value x^* is

$$\sigma \leq \sigma_c \equiv \max_x \{x [1 - P(x)]\} \quad (53)$$

Thus σ_c is the critical value of the external load per fiber, beyond which the bundle fails completely.

As a simple example take the uniform threshold distribution (2) with $x_r = 1$, for which the iterations take the form

$$x_{t+1} = \frac{\sigma}{1 - x_t} \quad \text{and} \quad U_{t+1} = 1 - \frac{\sigma}{U_t}. \quad (54)$$

Moreover, $\sigma_c = 1/4$, and the quadratic fixed-point equation for U^* has the solution

$$U^*(\sigma) = \frac{1}{2} \pm (\sigma_c - \sigma)^{1/2} = U^*(\sigma_c) \pm (\sigma_c - \sigma)^{1/2}, \quad (55)$$

since $U^*(\sigma_c) = 1/2$. The iterations are sketched in Fig. 11.

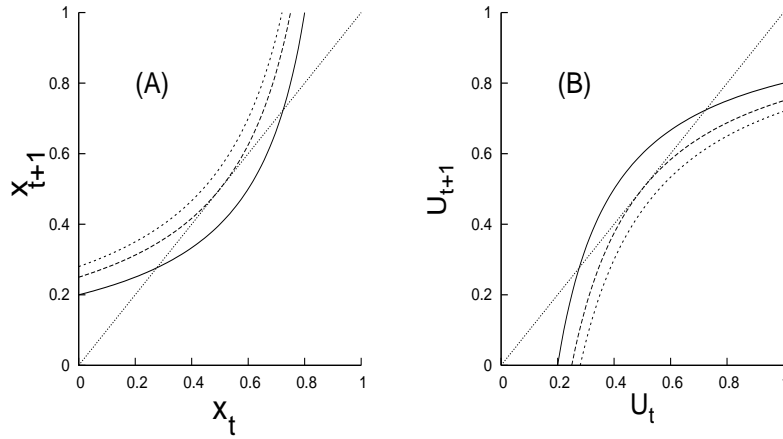


Fig. 11. Graphical representation of the iterations for x (A) and for U (B). The graphs are shown for different values of the external stress: $\sigma = 0.2$ (solid), 0.25 (dashed), and 0.28 (dotted), respectively. The intersections between the graph and the straight 45° line define possible fixed points.

A fixed point is attractive if $|dU_{t+1}/dU_t|$ is less than 1 at the fixed point and repulsive if the derivative exceeds unity. We see in Fig. 11 that the stable fixed point corresponds to the smallest value of x^* , and to the largest value of U^* (the plus sign in (55)):

$$U^*(\sigma) - U^*(\sigma_c) = (\sigma_c - \sigma)^\beta, \quad \text{with} \quad \beta = \frac{1}{2}. \quad (56)$$

Thus $U^*(\sigma) - U^*(\sigma_c)$ behaves like an order parameter, signalling total bundle failure when it is negative, partial failure when it is positive.

Close to a stable fixed point the iterated quantity changes with tiny amounts, so one may expand in the difference $\epsilon_t = U_t - U^*$. To first order (54) yields

$$\epsilon_{t+1} = \epsilon_t \cdot \frac{\sigma}{U^{*2}}. \quad (57)$$

Thus the fixed point is approached monotonously, with exponentially decreasing steps:

$$\epsilon_t \propto e^{-t/\tau}, \quad (58)$$

with

$$\tau = \frac{1}{\ln(U^{*2}/\sigma)}. \quad (59)$$

Precisely *at* the critical point, where $U^* = 1/2$ and $\sigma_c = 1/4$, the relaxation parameter τ is infinite, signalling a non-exponential approach to the fixed point. Close to the critical point one easily shows that

$$\tau \propto (\sigma_c - \sigma)^{-\alpha}, \quad \text{with } \alpha = \frac{1}{2}. \quad (60)$$

One may define a *breakdown susceptibility* χ by the change of $U^*(\sigma)$ due to an infinitesimal increment of the applied stress σ ,

$$\chi = -\frac{dU^*(\sigma)}{d\sigma} = \frac{1}{2}(\sigma_c - \sigma)^{-\gamma}, \quad \text{with } \gamma = \frac{1}{2}. \quad (61)$$

The susceptibility diverges as the applied stress σ approaches its critical value. Such a divergence was noted in previous numerical studies [19, 20].

When at criticality the approach to the fixed point is not exponential, what is it? Putting $U_t = U_c + \epsilon_t$ in the iteration (54) for $\sigma = 1/4$, it may be rewritten as follows

$$\epsilon_{t+1}^{-1} = \epsilon_t^{-1} + 2, \quad \text{with } \epsilon_0 = \frac{1}{2}, \quad (62)$$

with solution $\epsilon_t^{-1} = 2t + 2$. Thus we have, *exactly*,

$$U_t = \frac{1}{2} + \frac{1}{2t + 2}. \quad (63)$$

For large t this follows a power-law approach to the fixed point, $U_t - U_c = \frac{1}{2}t^{-\delta}$, with $\delta = 1$.

These critical properties are valid for the uniform distribution, and the natural question is how general the results are. In Ref. [18] two other threshold distributions were investigated, and all critical properties, quantified by the indices α, β, γ and δ were found to be the same as for the uniform threshold distribution. This suggests strongly that the critical behavior is universal, which we now prove.

When an iteration is close to the fixed point, we have for the deviation

$$\epsilon_{t+1} = U_{t+1} - U^* = P\left(\frac{\sigma}{U^*}\right) - P\left(\frac{\sigma}{U^* + \epsilon_t}\right) = \epsilon_t \cdot \frac{\sigma}{U^{*2}} p(\sigma/U^*), \quad (64)$$

to lowest order in ϵ_t .

This guarantees an exponential relaxation to the fixed point, $\epsilon_t \propto e^{-t/\tau}$, with parameter

$$\tau = 1 \left/ \ln \left(\frac{U^{*2}}{\sigma p(\sigma/U^*)} \right) \right. . \quad (65)$$

Criticality is determined by the extremum condition (8), which by the relation (48) takes the form

$$U_c^2 = \sigma p(\sigma/U_c)$$

Thus $\tau = \infty$ at criticality. To study the relaxation at criticality we must expand (64) to second order in ϵ_t since to first order we simply get the useless equation $\epsilon_{t+1} = \epsilon_t$. To second order we obtain

$$\epsilon_{t+1} = \epsilon_t - C\epsilon_t^2,$$

with a positive constant C . This is satisfied by

$$\epsilon_t = \frac{1}{Ct} + \mathcal{O}(t^{-2}).$$

Hence in general the dominating critical behavior for the approach to the fixed point is a power law with $\delta = 1$. The values $\alpha = \beta = \gamma = \frac{1}{2}$ can be shown to be consequences of the parabolic maximum of the load curve, (7) or (49), at criticality: $|x_c - x^*| \propto (\sigma_c - \sigma)^{\frac{1}{2}}$.

Thus all threshold distributions for which the macroscopic strength function has a single parabolic maximum, are in this universality class.

3 Fiber bundles with local load redistribution

The assumption that the extra stress caused by a fiber failure is shared equally among all surviving fibers is often unrealistic, since fibers in the neighborhood of the failed fiber are expected to take most of the load increase. One can envisage many systems for such local stress redistributions. A special case is the model with a one-dimensional geometry where the two nearest-neighbor fibers take up all extra stress caused by a fiber failure (Sec. 3.1). It is special for two reasons: It is an extreme case because the range of the stress redistribution is minimal, and, secondly, it is amenable to theoretical analysis. In other models, treated in Sec. 3.2 and 3.3, the stress redistribution occurs over a larger region. In Sec. 3.3 this comes about by considering a clamp to be an elastic medium.

3.1 Stress alleviation by nearest neighbors

The simplest model with nearest-neighbor stress redistribution is one-dimensional, with the N fibers ordered linearly, with or without periodic boundary conditions. Thus two fibers, one of each side, take up, and divide equally, the extra stress caused by a failure. The force on a fiber surrounded by n_l broken fibers on the left-hand side and n_r broken fibers on the right-hand side is then

$$\frac{F_{tot}}{N} \left(1 + \frac{1}{2}n_l + \frac{1}{2}n_r\right) \equiv f(2 + n_l + n_r), \quad (66)$$

where F_{tot} is the total force on the bundle, and $f = F_{tot}/2N$, one-half the force-per-fiber, is a convenient forcing parameter. The model has been discussed previously in a different context [21, 22, 23, 24, 25, 26]. Preliminary simulation studies [27, 28] showed convincingly that this local model is *not* in the same universality class as the equal-load-sharing fiber bundles. For the uniform threshold distribution and for $1 \leq \Delta \leq 10$ an effective exponent between 4 and 5 was seen, much larger than $5/2$.

Avalanches in this model, and in similar local stress-redistribution models, have a character different from bursts in the equal-load-sharing models. In the present model the failure of one fiber can by a domino effect set in motion a fatal avalanche: If the failing fiber has many previously failed fibers as neighbors, the load on the fibers on each side is high, and if they burst, the load on the new neighbors is even higher, etc., which may produce an unstoppable avalanche.

In Ref.[7] the burst distribution was determined analytically for the uniform threshold distribution,

$$P(x) = \begin{cases} x & \text{for } 0 \leq x \leq 1 \\ 1 & \text{for } x > 1 \end{cases} \quad (67)$$

In this model there is an upper limit to the size Δ of an avalanche that the bundle can survive. Since the threshold values are at most unity, it follows from (66) that if

$$\Delta > f^{-1} - 2, \quad (68)$$

then the bundle breaks down completely. Consequently an asymptotic power law distribution of the avalanche sizes is not possible.

In the analytic derivation periodic boundary conditions were used. The fairly elaborate procedure was based on a set of recursion relations between configurations and events at fixed external force. In Fig. 12 we show the resulting burst distribution for a bundle of $N = 20000$ fibers, compared with simulation results. The agreement is extremely satisfactory.

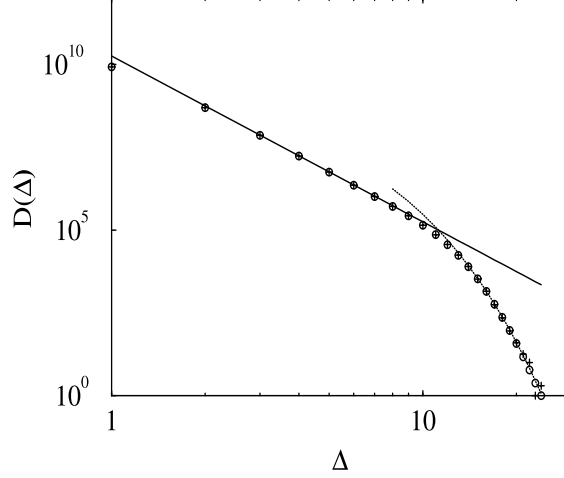


Fig. 12. Burst distribution in a local-load-sharing model for a bundle of $N = 20000$ fibers. Theoretical results are shown as circles, and simulation results (for 4000000 samples) are shown as crosses. The straight line shows the power law Δ^{-5} .

We see from Fig. 12 that, as expected, the burst distribution does *not* follow a power law for large Δ , but falls off faster. For Δ less than 10 the burst distribution follows approximately a power law, $D(\Delta) \propto \Delta^{-\xi}$ with ξ of the order of 5.

In Ref.[7] the maximum load F_{max} the fiber bundle could tolerate was estimated to have the following size dependence,

$$F_{max} \propto \frac{N}{\ln N}. \quad (69)$$

This is different from the equal-load-sharing model, for which $F_{max} \propto N$. A similar logarithmic size-dependence of the bundle strength for local-stress-redistribution models has been proposed by other authors [29, 30, 31].

The qualitative explanation of the non-extensive result is that for large N the probability of finding a weak region somewhere is high. Since, as discussed above, a weak region is the seed to complete bundle failure, it may be reasonable that the maximum load the bundle can carry does not increase proportional to N , but slower than linear.

3.2 Intermediate load-sharing models

It might be interesting to study models that interpolates between global and nearest-neighbor load sharing. The main question is whether the burst dis-

tribution changes from one behavior to the other in a continuous manner, or whether a discontinuous change occurs.

In Ref.[8] was introduced such an intermediate model, with the same one dimensional geometry as the nearest-neighbor model of the preceding section. When a fiber i fails in this model the elastic constants of the two nearest surviving neighbors l and r on both sides are updated as follows

$$\kappa_l \rightarrow \frac{1}{2}\lambda(\kappa_l + \kappa_r + \kappa_i) \quad (70)$$

$$\kappa_i \rightarrow 0 \quad (71)$$

$$\kappa_r \rightarrow \frac{1}{2}\lambda(\kappa_l + \kappa_r + \kappa_i). \quad (72)$$

For $\lambda = 1$ this corresponds to the local load-sharing by surviving nearest-neighbors (see the preceding section). And with $\lambda = 0$ the intact nearest-neighbor fibers to a failing fiber does not take part in the load-sharing. But since all the other surviving fibers then share the load equally, this limiting case must have the same behavior as the equal-load-sharing model. The numerics seems to suggest that there is a cross-over value of λ separating the universality classes of the local-load-sharing and the equal-load-sharing regimes.

A stress redistribution scheme that in a straightforward way interpolates between the two extreme models was recently proposed by Pradhan et al.[32]: A fraction g of the extra load caused by a fiber failure is shared by the nearest neighbors, and the remaining load is shared equally among all intact fibers. They show that in a one-dimensional geometry a crossover value g_c exists, such that for $g < g_c$ the bundle belongs to the equal-load-sharing regime, while for $g > g_c$ the system is like the local-load-sharing model of Sec. 3.1. The crossover value was determined to be $g_c = 0.79 \pm 0.01$.

It would be more realistic to have a stress redistribution whose magnitude falls off monotonically with the geometric distance r from the failed fiber. Hidalgo et al. [33] introduced such a model, for which the extra stress on a fiber followed a power law decay, proportional to $r^{-\gamma}$. In the limit $\gamma \rightarrow 0$ the equal-load-distribution model is recovered, while the limit $\gamma \rightarrow \infty$ corresponds to the nearest-neighbor model in Sec. 3.1. Again a crossover is observed, at a value $\gamma_c \simeq 2$ for the range parameter.

In the next section we consider a model with a different, but similar, interaction decaying with the distance from the failed fiber.

3.3 Elastic medium anchoring

In this section we generalize the fiber bundle problem to include more realistically the elastic response of the surfaces to which the fibers are attached. So far, these have been assumed to be infinitely stiff for the equal-load-sharing model, or their response has been modeled as very soft, but in a fairly unrealistic way in the local-load-sharing models, see Section 3.2. In [34], a realistic

model for the elastic response of the clamps was studied. The model was presented as addressing the problem of failure of weldings. In this context, the two clamps were seen as elastic media glued together at a common interface. Without loss of generality, one of the media was assumed to be infinitely stiff whereas the other was soft.

The two clamps can be pulled apart by controlling (fixing) either the applied force or the *displacement*. The displacement is defined as the change in the distance between two points, one in each clamp positioned far from the interface. The line connecting these points is perpendicular to the average position of the interface. In our case, the pulling is accomplished by controlling the displacement. As the displacement is increased slowly, fibers — representing the glue — will fail, ripping the two surfaces apart.

The model consists of two two-dimensional square $L \times L$ lattices with periodic boundary conditions. The lower one represents the hard, stiff surface and the upper one the elastic surface. The nodes of the two lattices are matched (*i.e.* there is no relative lateral displacement). The thresholds of the fibers are taken from an uncorrelated uniform distribution. The spacing between the fibers is a in both the x and y directions. The force that each fiber is carrying is transferred over an area of size a^2 to the soft clamp: As the two clamps are separated by controlling the displacement of the hard clamp, D , the forces carried by the fibers increase. As for the fiber bundle models studied in the previous sections, when the force carried by a fiber reaches its breaking threshold, it breaks irreversibly and the forces redistribute. Hence, the fibers are broken one by one until the two clamps are no longer in mechanical contact. As this process is proceeding, the elastic clamp is of course deforming to accomodate the changes in the forces acting on it.

The equations governing the system are as follows. The force, f_i , carried by the i th fiber is given by

$$f_i = -k(u_i - D) , \quad (73)$$

where k is the spring constant and u_i is the deformation of the elastic clamp at site i . All unbroken fibers have $k = 1$ while a broken fiber has $k = 0$. The quantity $(u_i - D)$ is, therefore, the length fiber i is stretched. In addition, a force applied at a point on an elastic surface will deform this surface over a region whose extent depends on its elastic properties. This is described by the coupled system of equations,

$$u_i = \sum_j G_{i,j} f_j , \quad (74)$$

where the elastic Green function, $G_{i,j}$ is given by [35, 36]

$$G_{i,j} = \frac{1 - s^2}{\pi e a^2} \int_{-a/2}^{+a/2} \int_{-a/2}^{+a/2} \frac{dx' dy'}{|(x - x', y - y')|} . \quad (75)$$

In this equation, s is the Poisson ratio, e the elastic constant, and the denominator $|\mathbf{i} - \mathbf{j}|$ is the distance between sites $i = (x, y)$ and $j = (x', y')$. The indices i and j run over all L^2 sites. The integration over the area a^2 is done to average the force from the fibers over this area. Strictly speaking, the Green function applies for a medium occupying the infinite half-space. However, with a judicious choice of elastic constants, we may use it for a finite medium if its range is small compared to L , the size of the system.

By combining equations (73) and (74), we obtain

$$(\mathbf{I} + \mathbf{K}\mathbf{G})\mathbf{f} = \mathbf{K}\mathbf{D}, \quad (76)$$

where we are using matrix-vector notation. \mathbf{I} is the $L^2 \times L^2$ identity matrix, and \mathbf{G} is the Green function represented as an $L^2 \times L^2$ dense matrix. The constant vector \mathbf{D} is L^2 dimensional. The *diagonal* matrix \mathbf{K} is also $L^2 \times L^2$. Its matrix elements are either 1, for unbroken fibers, or 0 for broken ones. Of course, \mathbf{K} and \mathbf{G} do not commute.

Once equation (76) is solved for the force \mathbf{f} , equation (74) easily yields the deformations of the elastic clamp.

Equation (76) is of the familiar form $\mathbf{A}\mathbf{x} = \mathbf{b}$. Since the Green function connects all nodes to all other nodes, the $L^2 \times L^2$ matrix \mathbf{A} is dense which puts severe limits on the size of the system that may be studied.

The simulation proceeds as follows: We start with all springs present, each with its randomly drawn breakdown threshold. The two clamps are then pulled apart, the forces calculated using the Conjugate Gradient (CG) algorithm [37, 38], and the fiber which is the nearest to its threshold is broken, *i.e.* the corresponding matrix element in the matrix \mathbf{K} is zeroed. Then the new forces are calculated, a new fiber broken and so on until all fibers have failed.

However, there are two problems that render the simulation of large systems extremely difficult. The first is that since \mathbf{G} is a $L^2 \times L^2$ *dense* matrix, the number of operations per CG iteration scales like L^4 . Even more serious is the fact that as the system evolves and springs are broken, the matrix $(\mathbf{I} + k\mathbf{G})$ becomes very ill-conditioned.

To overcome the problematic L^4 scaling of the algorithm, we note that the Green function is diagonal in Fourier space. Consequently, doing matrix-vector multiplications using FFTs the scaling is much improved and goes like $L^2 \ln(L)$. Symbolically, this can be expressed as follow:

$$(\mathbf{I} + \mathbf{K}\mathbf{F}^{-1}\mathbf{F}\mathbf{G})\mathbf{F}^{-1}\mathbf{F}\mathbf{f} = \mathbf{K}\mathbf{D}, \quad (77)$$

where \mathbf{F} is the FFT operator and \mathbf{F}^{-1} its inverse ($\mathbf{F}^{-1}\mathbf{F} = 1$). Since \mathbf{I} and \mathbf{K} are diagonal, operations involving them are performed in real space. With this formulation, the number of operations/iteration in the CG algorithm now scales like $L^2 \ln(L)$.

To overcome the runaway behavior due to the ill-conditioning we need to precondition the matrix [37, 39]. This means that instead of solving equation (77), we solve the equivalent problem

$$\mathbf{Q}(\mathbf{I} + \mathbf{K}\mathbf{F}^{-1}\mathbf{F}\mathbf{G})\mathbf{F}^{-1}\mathbf{F}\mathbf{f} = \mathbf{Q}\mathbf{K}\mathbf{D}, \quad (78)$$

where we simply have multiplied both sides by the arbitrary, positive definite preconditioning matrix \mathbf{Q} . Clearly, the ideal choice is $\mathbf{Q}_0 = (\mathbf{I} + \mathbf{K}\mathbf{G})^{-1}$ which would always solve the problem in one iteration. Since this is not possible in general, we look for a form for \mathbf{Q} which satisfies the following two conditions: (1) It should be as close as possible to \mathbf{Q}_0 , and (2) be fast to calculate. The choice of a good \mathbf{Q} is further complicated by the fact that as the system evolves and fibers are broken, corresponding matrix elements of \mathbf{K} are set to zero. So, the matrix $(\mathbf{I} + \mathbf{K}\mathbf{G})$ evolves from the initial form $(\mathbf{I} + \mathbf{G})$ to the final one \mathbf{I} .

Batrouni et al. [34] chose the form

$$\mathbf{Q} = \mathbf{I} - (\mathbf{K}\mathbf{G}) + (\mathbf{K}\mathbf{G})(\mathbf{K}\mathbf{G}) - (\mathbf{K}\mathbf{G})(\mathbf{K}\mathbf{G})(\mathbf{K}\mathbf{G}) + \dots \quad (79)$$

which is the Taylor series expansion of $\mathbf{Q}_0 = (\mathbf{I} + \mathbf{K}\mathbf{G})^{-1}$. For best performance, the number of terms kept in the expansion is left as a parameter since it depends on the physical parameters of the system. It is important to emphasize the following points: (a) As fibers are broken, the preconditioning matrix evolves with the ill-conditioned matrix and, therefore, remains a good approximation to its inverse throughout the breaking process. (b) All matrix multiplications involving \mathbf{G} are done using FFTs. (c) The calculation of \mathbf{Q} can be easily organized so that it scales like $nL^2 \ln(L)$ where n is the number of terms kept in the Taylor expansion, equation (79). The result is a stable accelerated algorithm which scales essentially as the volume of the system.

Fig. 13 (left) shows the force-displacement curve for a system of size 128×128 with elastic constant $e = 10$. Whether we control the applied force, F , or the displacement, D , the system will eventually suffer catastrophic collapse. However, this is not so when $e = 100$ as shown in Fig. 13 (right). In this case, only controlling the force will lead to catastrophic failure. In the limit when $e \rightarrow \infty$, the model becomes the equal-load-sharing fiber bundle model, where $F = (1 - D)D$. In this limit there are no spatial correlations and the force instability is due to the decreasing total elastic constant of the system making the force on each surviving bond increase faster than the typical spread of threshold values. No such effect exists when controlling displacement D . However, when the elastic constant, e , is small, spatial correlations in the form of localization, where fibers that are close in space have a tendency to fail consecutively, do develop, and these are responsible for the displacement instability which is seen in Fig. 13.

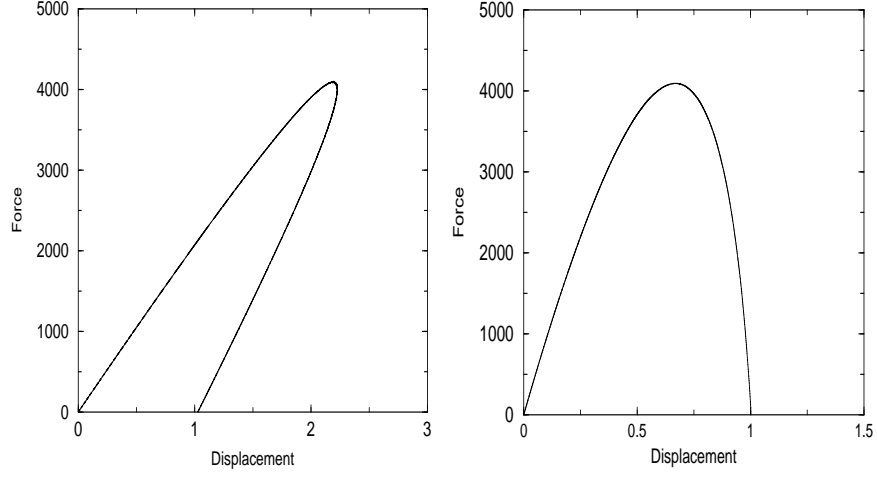


Fig. 13. Force-displacement curve, 128×128 systems with $e = 10$ (left) and $e = 100$ (right).

We now turn to the study of the burst distribution. We show in Fig. 14 the burst distributions for $e = 10$ and $e = 100$. In both cases we find that the burst distribution follows a power law with an exponent $\xi = 2.6 \pm 0.1$. It was argued in Ref. [34] that the value of ξ in this case is indeed $5/2$ as in the global-load-sharing model.

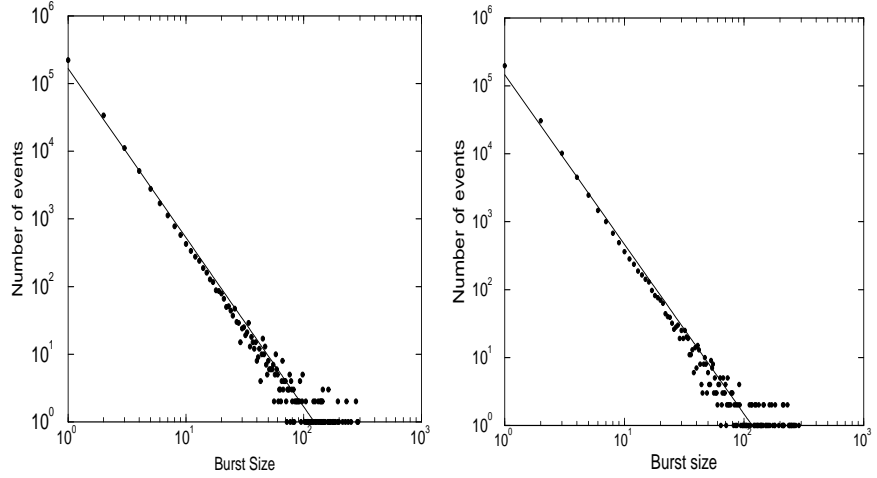


Fig. 14. Burst distribution for 128×128 , for $e = 10$ (left) and $e = 100$ (right). The slope of the straight lines is -2.5 .

As the failure process proceeds, there is an increasing competition between global failure due to stress enhancement and local failure due to local weakness of material. When the displacement, D , is the control parameter and e is sufficiently small (for example $e = 10$), catastrophic failure eventually occurs due to localization. The onset of this localization, *i.e.* the catastrophic regime, occurs when the two mechanisms are equally important. This may be due to self organization [40] occurring at this point. In order to test whether this is the case, Batrouni et al. [34] measured the size distribution of broken bond clusters at the point when D reaches its maximum point on the $F - D$ characteristics, *i.e.* the onset of localization and catastrophic failure. The analysis was performed using a Hoshen-Kopelman algorithm [41]. The result is shown in Fig. 15, for 56 disorder realizations, $L = 128$ and $e = 10$. The result is consistent with a power law distribution with exponent -1.6 , and consequently with self organization. If this process were in the universality class of percolation, the exponent would have been -2.05 . Hence, we are dealing with a new universality class in this system.

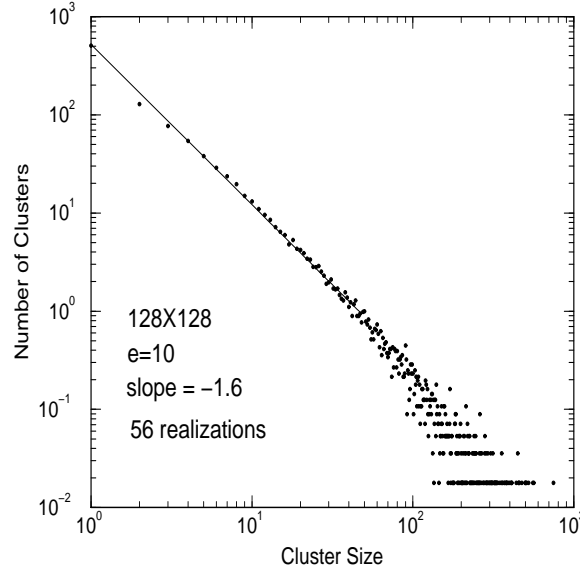


Fig. 15. Area distribution of zones where glue has failed for systems of size 128×128 and elastic constant $e = 10$. The straight line is a least square fit and indicates a power law with exponent -1.6 .

Acknowledgment: S. P. thanks NFR (Research Council of Norway) for financial support through Grant No. 166720/V30.

References

1. H. J. Herrmann and S. Roux, eds. *Statistical Models for the Fracture of Disordered Media* (North-Holland, Amsterdam, 1990).
2. B. K. Chakrabarti and L. G. Benguigui *Statistical Physics and Breakdown in Disordered Systems* (Oxford University Press, Oxford, 1997).
3. D. Sornette *Critical Phenomena in Natural Sciences* (Springer Verlag, Berlin, 2000).
4. H. E. Daniels, Proc. Roy. Soc. London **A183**, 405 (1945).
5. P. C. Hemmer and A. Hansen, ASME J. Appl. Mech. **59**, 909 (1992).
6. F. T. Peirce, J. Text. Ind. **17**, 355 (1926).
7. M. Kloster, A. Hansen, and P. C. Hemmer, Phys. Rev. E, **56**, 2615 (1997).
8. A. Hansen and P. C. Hemmer, Trends in Statistical Physics **1**, 213 (1994).
9. W. Lee, Phys. Rev. B **50**, 3797 (1994).
10. S. Pradhan, A. Hansen, and P. C. Hemmer, Phys. Rev. Lett. **95**, 125501 (2005).
11. S. Pradhan, A. Hansen, and P. C. Hemmer, submitted to Phys. Rev. E, cond-mat/0512015 (2005).
12. D. Sornette, J. Phys. I France **4**, 209 (1994).
13. S. Zapperi, P. K. V. V. Nukula, and S. Simunovic, Phys. Rev. E. **71**, 026106 (2005).
14. H. Kawamura, arXiv:cond-mat/0603335, (2006).
15. R. de Silveira, Am. J. Phys. **67**, 1177 (1999).
16. S. Pradhan and B. K. Chakrabarti, Phys. Rev. E **65**, 016113 (2001).
17. S. Pradhan, P. Bhattacharyya, and B. K. Chakrabarti, Phys. Rev. E **66** 016116 (2002).
18. P. Bhattacharyya, S. Pradhan, and B. K. Chakrabarti, Phys. Rev. E **67**, 046122 (2003).
19. S. Zapperi, P. Ray, H. E. Stanley, and A. Vespignani, Phys. Rev. Lett. **85**, 2865 (2000).
20. R. de Silveira, Am. J. Phys. **67**, 1177 (1999).
21. D. G. Harlow, Proc. Roy. Soc. Lond. Ser. A **397**, 211 (1985).
22. D. G. Harlow and S. L. Phoenix, J. Mech. Phys. Solids **39**, 173 (1991).
23. P. M. Duxbury and P. M. Leath, Phys. Rev. B **49**, 12676 (1994).
24. D. G. Harlow and S. L. Phoenix, Int. J. Fracture **17**, 601 (1981).
25. S. L. Phoenix and R. L. Smith, Int. J. Sol. Struct. **19**, 479 (1983).
26. C. C. Kuo and S. L. Phoenix, J. Appl. Prob. **24**, 137 (1987).
27. A. Hansen and P. C. Hemmer, Phys. Lett. A **184**, 394 (1994).
28. S. D. Zhang and E. J. Ding, Phys. Lett. A **193** 425 (1994).
29. R. L. Smith, Ann. Prob. **10**, 137 (1982).
30. S. D. Zhang and E. J. Ding, Phys. Rev. B **53**, 646 (1996).
31. S. D. Zhang and E. J. Ding, J. Phys. A **28**, 4323 (1995).
32. S. Pradhan, B. K. Chakrabarti, and A. Hansen, Phys. Rev. E **71**, 036149 (2005).
33. R. C. Hidalgo, Y. Moreno, F. Kun, and H. J. Herrmann, Phys. Rev. E **65**, 046148 (2002).
34. G. G. Batrouni, A. Hansen, and J. Schmittbuhl, Phys. Rev. E **65**, 036126 (2002).
35. L. Landau and E. M. Lifshitz, *Theory of Elasticity* (Clarendon Press, Oxford, 1958).
36. K. L. Johnson, *Contact Mechanics* (Cambridge University Press, Cambridge, 1985).

- 37. G. G. Batrouni and A. Hansen, J. Stat. Phys. **52**, 747 (1988).
- 38. W. H. Press, S. A. Teukolsky, W. T. Vetterling, and B. P. Flannery, *Numerical Recipes in Fortran 77: The Art of Scientific Computing* (Cambridge University Press, Cambridge, 1992).
- 39. G. G. Batrouni, A. Hansen, and M. Nelkin, Phys. Rev. Lett. **57**, 1336 (1986).
- 40. P. Bak, C. Tang and K. Wiesenfeld, Phys. Rev. Lett. **59**, 381 (1987).
- 41. D. Stauffer and A. Aharony, *Introduction to Percolation Theory* (Taylor and Francis, London, 1992).